High-temperature ferroic phase transitions and paraelectric cubic phase in multiferroic Bi0.951dFe0.9Zr0.1O3

Wei Jie, R. Haumont, R. Jarrier, P. Berthet, B. Dkhil

High-temperature ferroic phase transitions and paraelectric cubic phase in multiferroic $Bi_{0.95+\delta}Fe_{0.9}Zr_{0.1}O_3$

Jie Wei,[1,2,a)] Raphael Haumont,[2,3] Romain Jarrier,[2,3] Patrick Berthet,[2] and Brahim Dkhil[3]
[1]*Electronic Materials Research Laboratory, Key Laboratory of Ministry of Education, Xi'an Jiaotong University, Xi'an 710049, China*
[2]*Laboratoire de Physico-Chimie de l'Etat Solide, ICMMO, CNRS-UMR 8182, Bâtiment 410, Université Paris-Sud XI, 15 rue Georges Clémenceau, 91405 Orsay Cedex, France*
[3]*Laboratoire Structures, Propriétés et Modélisation des Solides, CNRS-UMR8580, Ecole Centrale Paris, Grande Voie des Vignes, 92295 Chatenay-Malabry Cedex, France*

(Received 19 March 2012; accepted 12 May 2012; published online 14 June 2012)

The temperature-dependent phase transitions of $Bi_{0.95+\delta}Fe_{0.9}Zr_{0.1}O_3$ have been studied using high-temperature x-ray powder diffraction together with differential scanning calorimetry measurements. The results show that $Bi_{0.95+\delta}Fe_{0.9}Zr_{0.1}O_3$ undergoes two phase transitions at 815 °C and 905 °C before decomposition at 920 °C. It appears that Zr-doping seems to stabilize the high temperature phases in such compound. Both the sharp contraction in the unit-cell volume and enthalpy thermal hysteresis demonstrate that the ferroelectric phase transition ($\alpha \leftrightarrow \beta$) at 815 °C is of first order nature. In contrast, the highest $\beta \leftrightarrow \gamma$ phase transition at 905 °C appears to be a second-order-like one. The analysis of the diffraction pattern in addition to Rietveld refinement strongly suggests a cubic symmetry for γ-phase. © *2012 American Institute of Physics*. [http://dx.doi.org/10.1063/1.4729484]

I. INTRODUCTION

Multiferroic materials, which show simultaneous ferroelectric and magnetic ordering, have been attracting tremendous interest due to the promising multifunctional device applications and interest in the fundamental physics as well.[1–3] Among them, $BiFeO_3$ (BFO), that is considered as the prototypical multiferroic oxide with the perovskite structure (ABO_3), is intensively studied due to its relatively high Neel temperature ($T_N \sim 370$ °C) and Curie temperature ($T_C \sim 820$ °C).[4,5] At ambient conditions, the BFO phase is described by the rhombohedral $R3c$ space group, which allows antiphase octahedral tilting and ionic displacements from the centrosymmetric positions about and along, respectively, a same $\langle 111 \rangle$ cubic-like direction,[6] In addition to the G-type antiferromagnetic spin ordering,[7] a cycloid-type spatial spin modulation[8] occurs below the Néel temperature. It is believed that such spiral modulation prevents the observation of an intrinsic and weak ferromagnetic moment driven by Dzyaloshinsky-Moriya (DM) interactions, which, in turn, results in a poor linear magnetoelectric effect. Room temperature structure and properties of BFO ceramics and thin films have been extensively investigated,[4–13] while studies of the ferroic phase transitions remain scarce.

The critical temperatures of the two ferroic phase transitions in BFO,[14] from antiferromagnetism to paramagnetism and from α ferroelectric phase to β paraelectric phase, are known to occur at $T_N \sim 370$ °C and $T_C \sim 820$ °C, respectively. However, while the crystalline structure of the α phase is clearly identified, that of the paraelectric β phase is still unclear because of the volatility of Bi at high temperature and the techniques used as for instance neutron diffraction is more sensitive to oxygen atom positions compared to x-ray diffraction (XRD). Several different symmetries and space groups as cubic $Pm\bar{3}m$, rhombohedral $R3m$ or $R\bar{3}c$, orthorhombic $Pbnm$ or $P2mm$, tetragonal $I4/mcm$, and monoclinic $P2_1/m$ phase have been proposed.[14–20] Furthermore, at higher temperature, Palai *et al.*[17] have reported, on the basis of Raman scattering studies, the existence of a cubic γ phase at 925 °C, just below the peritectic decomposition temperature T_{per} of about 935 °C. These authors have suggested a second-order-like transition, accompanied by a metal-insulator transition also observed at high pressure.[21,22] However, the vicinity of the phase transition at 925 °C to the peritectic temperature has hampered structural studies of the cubic polymorph and other research groups observed decomposition of BFO before reaching this phase. The decomposition of BFO above T_c is one of the main reasons explaining the different structures determined for β phase and the difficulty or impossibility to observe the γ phase. The high temperature instability due to bismuth volatility gives rise to parasitic second phases like $Bi_{25}FeO_{39}$ and $Bi_2Fe_4O_9$ even just above 820 °C. Note that the strong volume change[17,20] at T_C might also participate to the destabilization of the structure as this first-order-like phase transition requires phases coexistence with both compressive/tensile stresses and thermal energy exchanges.

Several attempts[23–25] have been made to stabilize the crystal structure of BFO at high temperature by doping BFO. Recently, we reported on the synthesis and properties of Zr doped BFO.[26] Strikingly, in contrast to other doped BFO compounds, both the crystalline structure and Curie temperature T_C are not changed which makes Zr-doped BFO system of interest to reveal the intrinsic phase transitions of BFO. In this paper, we report on the temperature-dependent phase transitions of $Bi_{0.95+\delta}Fe_{0.9}Zr_{0.1}O_3$ (BFZ_{95}) powder. In addition to the Curie and Néel phase transitions, the β- to γ-phase transition is also observed revealing a cubic-like symmetry for γ-phase.

a)Author to whom correspondence to should be addressed. Electronic mail: weij2008@mail.xjtu.edu.cn.

II. EXPERIMENTAL TECHNIQUES AND SAMPLE PREPARATION

$Bi_XFe_{0.9}Zr_{0.1}O_3$ ($x = 0.95$, 0.975, 1) ceramics were prepared by an improved solid-state reaction[26] using high-purity bismuth oxide Bi_2O_3, iron oxide Fe_2O_3, and zirconium 2, 4-pentanedionate $Zr(O_2C_5H_7)_4$ powders. XRD patterns from $2\theta = 5°$ to 120° with a step of 0.04° were collected with a Philips X-celerator Bragg-Brentano diffractometer equipped with a copper source ($\lambda = 1.54056$ Å). The patterns were recorded from 25 °C to 1000 °C under air atmosphere by using a furnace with accuracy better than 2 °C. Rietveld refinements were performed using XND analysis program.[27] Differential scanning calorimetry (DSC) (Setaram Labsys DSC) was used to follow the phase transformations involved up to 1000 °C with a heating/cooling rate of 2.5 °C/min. Indeed, any appearance of endothermic/exothermic peaks is related to either structural or phase change. Note that to check the reversibility of the processes several heating/cooling cycles were performed.

III. RESULTS

Attempts to synthesis $BiFe_{0.9}Zr_{0.1}O_3$ (BFZ_{100}) ceramic reveal that it is impossible to obtain the pure phase even if the sintering temperature is increased upon 880 °C using a rapid liquid sintering technology.[28] Indeed, doping with non-isovalent ions can result in the appearance of impurities and thus addition of Zr^{4+} ions into BFO host crystal requires charge compensation, which can be achieved by one, or more, of the following mechanisms: (1) filling of the intrinsic oxygen vacancies; (2) change of cation valence, i.e., formation of Fe^{2+}; (3) creation of cation vacancies.[29]

In our case, we rather favored cation vacancies of Bi^{3+} by reducing the content of Bi, and finally, we prepared $Bi_XFe_{0.9}Zr_{0.1}O_3$ ($x = 1$, 0.975, 0.95) ceramics. Figure 1 shows the room temperature XRD patterns of the sintered $Bi_XFe_{0.9}Zr_{0.1}O_3$ ($x = 1$, 0.975, 0.95) ceramics. As seen in Fig. 1, some impurities appear in the samples $BiFe_{0.9}Zr_{0.1}O_3$ (BFZ_{100}) and $Bi_{0.975+\delta}Fe_{0.9}Zr_{0.1}O_3$ ($BFZ_{97.5}$, "δ" represents the cation vacancies). However, the amount of impurities apparently decreases with the content of Bi. When $x = 0.95$, i.e., $Bi_{0.95+\delta}Fe_{0.9}Zr_{0.1}O_3$ (BFZ_{95}), the pure phase is achieved. According to JCPDS card No. 86-1518, the XRD analysis shows that the BFZ_{95} ceramic is a single-phase perovskite compound with the same structure as that of the parent BFO. It is worth mentioning that the major phase in BFZ_{100} and $BFZ_{97.5}$ ceramics has the same structure as that of BFZ_{95}, which implies that the substitution of Zr^{4+} does not affect the structure of BFO. In addition, these XRD results confirm that doping BFO by Zr^{4+} ions creates cation vacancies in the $Bi_XFe_{0.9}Zr_{0.1}O_3$ ceramics as expected for charge compensation.

For each Bi content, we performed a Rietveld refinement by using XND software. The table inset of Fig. 1 shows the variation of the perovskite unit cell parameters versus the content of Bi in $Bi_XFe_{0.9}Zr_{0.1}O_3$ ($x = 1$, 0.975, 0.95) ceramics. With decreasing Bi content, both *a* and *c* parameters decrease, leading to the diminution of the unit cell volume. These results confirm the existence of cation vacancies and highlights that the concentration of cation vacancies (Bi^{3+}) in the $Bi_XFe_{0.9}Zr_{0.1}O_3$ (BFZ_X) ceramics increases by reducing the content of Bi. In spite of the decrease of both *a* and *c* parameters, the *c*/*a* ratio remains almost unaffected which may explain that $Bi_XFe_{0.9}Zr_{0.1}O_3$ compounds keep the same crystalline structure as that of the parent BFO.

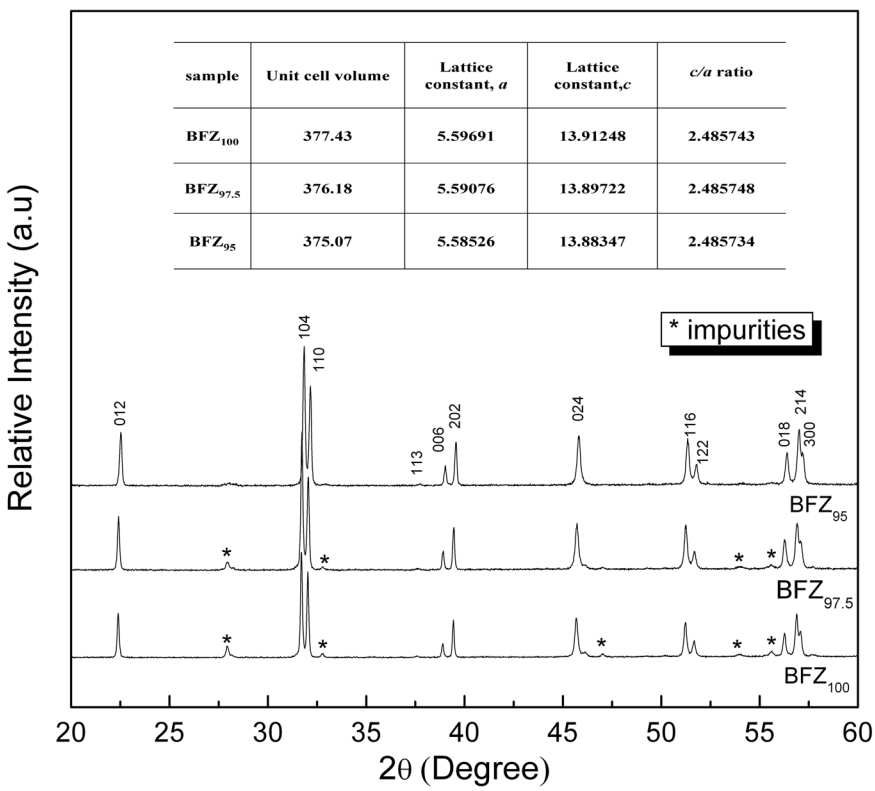

FIG. 1. X-ray diffraction patterns of $Bi_XFe_{0.9}Zr_{0.1}O_3$ ($x = 1$, 0.975, 0.95) ceramics (table inset sums up cell parameters).

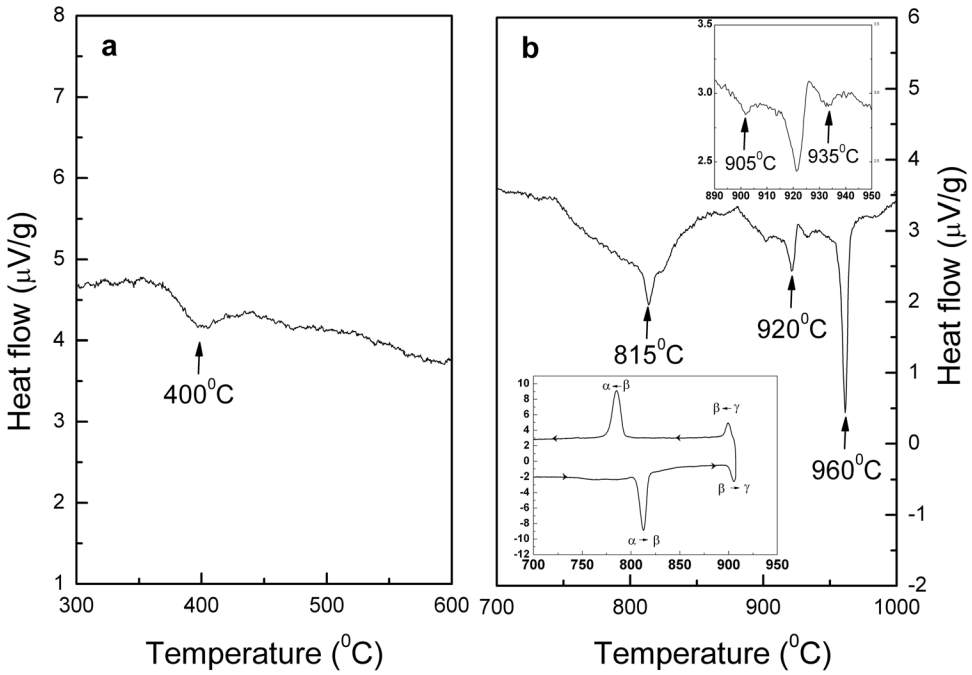

FIG. 2. DSC signal versus temperature in the $Bi_{0.95+\delta}Fe_{0.9}Zr_{0.1}O_3$ ceramic (up inset of (b): zoom around the first decomposition temperature; down inset of (b): zoom around the ferroelectric transition at 820 °C versus increasing and decreasing temperatures).

We now turn our attention to the high temperature phase evolutions of pure phase BFZ_{95} ceramic.

Figure 2 shows the DSC data of BFZ_{95} ceramic recorded during the heating process. In addition, in order to better understand the transformations stressed by the DSC measurements, we recorded high temperature x-ray diffraction (HTXRD) patterns of BFZ_{95} ceramic from room temperature till 1000 °C under air atmosphere as illustrated in Fig. 3. We can see four obvious endothermic peaks in the DSC curves, which can be identified at 400 °C, 815 °C, 920 °C, and 960 °C. The four peaks are in agreement with our previous report[20] on the phase transitions of pure BFO. The two endothermic peaks at 400 °C and 815 °C in the DSC curves correspond to the magnetic (T_N) and ferroelectric (T_C) phase transition temperatures, respectively. T_C is very close to that of pure BFO, attesting that doping by Zr does not disturb this transition. However, T_N is a little bit higher than that of pure BFO showing that Fe replacement by non-magnetic ions as Zr effects the magnetic ordering as it was discussed previously.[26]

On heating above T_C, an irreversible decomposition occurs at 920 °C and is characterized by the loss of the BFZ_{95} diffraction peaks against the appearance of $Bi_2Fe_{4-y}Zr_yO_9$ compounds accompanied with few amount of $Zr_{0.932}O_3$ and Fe_2O_3 phases (pattern D of Fig. 3). This transformation is

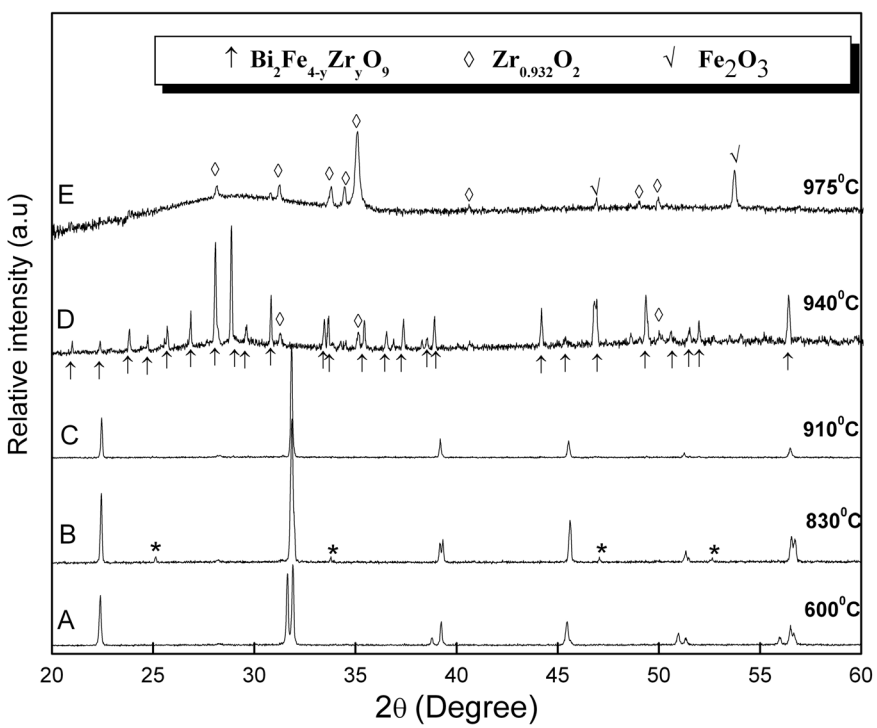

FIG. 3. X-ray diffraction patterns of BFZ_{95} ceramic recorded under different temperatures (asterisk: weak diffraction peaks observed in the diffraction pattern recorded at 830 °C).

clearly seen in the DSC curve (Fig. 2(b)). The compounds $Bi_2Fe_{4-y}Zr_yO_9$ with its parent phase $Bi_2Fe_4O_9$ are the main parasitic phases, which appear during the sintering process at rather high temperature. It is worth noting that such parasitic phases can also appear already at 880 °C, i.e., below the decomposition temperature of 920 °C, after long-time annealing treatment, showing that the kinetic is a key parameter that should be taken into account in such measurements. At 960 °C, another strong endothermic peak occurs and corresponds to a peritectic plateau. Above 960 °C, the diffraction pattern (pattern E in Fig. 3(a)) displays the complete transformation of $Bi_2Fe_{4-y}Zr_yO_9$ into liquid coexisting with $Zr_{0.932}O_3$, Fe_2O_3 phases.

Nonetheless, a careful inspection of the DSC curve shows two weak but significant peaks at 905 °C and 935 °C, respectively, on both sides of the first decomposition temperature at 920 °C (upper inset of Fig. 2(b)). To clarify the existence of these subtle changes at high temperature, we performed another DSC measurement by recording the heating/cooling processes between 700 °C and the first decomposition temperature (inset at the bottom of Fig. 2(b)). The first endothermic peak occurring at 815 °C corresponds to the expected Curie temperature (T_C). A reversible exothermic peak with almost same intensity/area than the endothermic one appears at 790 °C during the cooling process, which implies that this ferroelectric phase transition is of first-order. An additional obvious endothermic peak appears on heating close to 905 °C with a corresponding reversible exothermic peak having almost the same intensity as the endothermic one appears at 902 °C during the cooling process. This result indicates that there is another phase transition above T_C which is of second-order or at least weakly of first-order. The diffraction pattern C in Fig. 3 recorded at 910 °C attests on the existence of a new phase which compared to β-phase (pattern B in Fig. 3) has no superstructure peaks (asterisks in Fig. 3) and no splitting of the main Bragg peaks. At a first-glance, this new phase has a cubic symmetry and corresponds to the γ-phase. Figure 4 shows a focus on the (110) pseudo-cubic Bragg peak as a function of temperature. The α- to β- and γ-phase transitions are clearly seen by the successive change of splitting until the Bragg peak becomes single with a narrower width in the γ-phase. For the other weak endothermic peak occurring at 935 °C, we argue that it may correspond to the decomposition of residual perovskite-like phase.

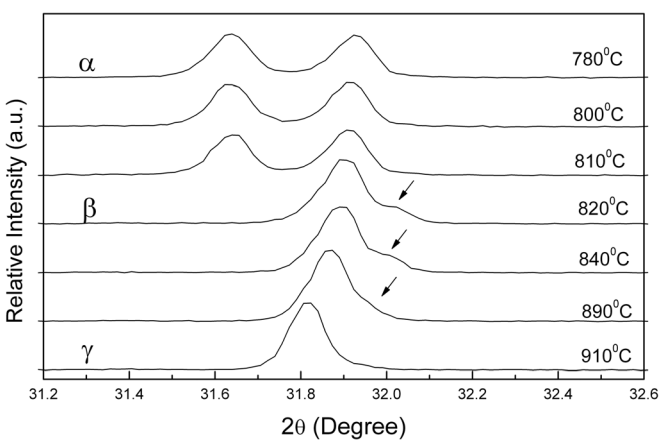

FIG. 4. HTXRD patterns of BFZ_{95} ceramic at selected temperatures, focusing on the resolution of the pseudocubic $(110)_c$ reflection through the $\alpha \leftrightarrow \beta \leftrightarrow \gamma$ phase transitions.

Below the Curie temperature T_C, the structure is well described by *R3c* space group. Concerning the phase above T_C, we have performed a Rietveld analysis for each diffraction pattern recorded below 900 °C, by using the XND software. Each diffraction pattern is refined using pseudo-Voigt peak-shape function including asymmetric broadening, linear interpolation for the background, and isotropic thermal factors (as seen in Table I). Because some weak peaks are evidenced in the diffraction pattern recorded at 830 °C (see asterisks in pattern B of Fig. 3), it is impossible to well describe the whole diffraction pattern just using the classical perovskite symmetries (including cubic $Pm\bar{3}m$, tetragonal *P4mm*, orthorhombic *Bmm2*, rhombohedral *R3m*, and monoclinic *Cm* or *Pm* phases). As reported in our previous paper,[20] we have carefully indexed all the observed superstructure reflections. Using the double perovskite unit cell, we found that these weak peaks correspond to [*oee*] reflections (where *o* and *e* are *odd* and *even* Miller indexes, respectively), involving the presence of clockwise and counter clockwise oxygen octahedra rotation. As the above T_c phase is expected to be paraelectric, centrosymmetric space groups in agreement with such tilt systems (*Cmcm, Pbnm,* $P2_1/m$*, and* $P4_2/nmc$) were tested by Rietveld refinements. Consequently, the best agreement matching between the observed and calculated profiles is obtained with the monoclinic $P2_1/m$ space group (Space Group SG no. 11 of the International Tables of Crystallography[30]) with constrained oxygen atom positions (the lattice parameters recorded at 830 °C are $a_M = 5.6341(1)$ Å, $b_M = 7.9988(3)$ Å, $c_M = 5.6642(1)$ Å, $\gamma = 90.010(3)^0$, as seen in Table I). Moreover, this space group is centrosymmetric, which implies that the phase is not ferroelectric. This result shows that the crystal structure of BFZ_{95} ceramic between T_C and 905 °C has a similar symmetry as that of the pure BFO reported in our previous paper.[20] It is worth recalling that here the experiments are done using an x-ray source which implies a stronger interaction with heavy atoms as Bi, Fe, and Zr while the light oxygen atom positions should be better described using interaction with neutron radiation. As a result, the refined structure is not complete and needs further experiment to fully describe the real structure. Nonetheless, using this set of experiment, we can show that the β-phase of BFZ_{95} is well described by the space group used for β-phase of pure BFO.

For the new γ-phase existing between 905 °C and 920 °C, we also performed a Rietveld analysis for the diffraction pattern recorded at 910 °C by using the XND software. The result shows that the structure is well described by a cubic $Pm\bar{3}m$ space group (Space Group SG no. 221 of the International Tables of Crystallography[30]) which gives a lattice parameter of $a_C = 4.0041(3)$ Å at 910 °C, as seen in Table I.

The pseudo-cubic lattice parameters of BFZ_{95} ceramic, i.e., a_h and c_h in hexagonal cell for α-phase ($a_h = a_H/\sqrt{2}$,

TABLE I. Results of Rietveld x-ray diffraction refinements on BFZ_{95} at 25 °C, 830 °C, and 910 °C.

	BFZ_{95}−25 °C-$R3c$	BFZ_{95}−830 °C-$P2_1/m$			BFZ_{95}−910 °C-$Pm-3m$
Lattice parameters					
a(Å)	5.5852(6)	5.6341(1)			
b(Å)	5.5852(6)	7.9988(3)			4.0041(3)
c(Å)	13.8834(7)	5.6642(1)			
		γ (^{0}): 90.010(3)			
Position of Bi					
x	0	0	1/2		0
y	0	0	0		0
z	0	0	1/2		0
$B_{eq(Bi)}$(Å^2)	2.22	5.86	5.86		7.56
Position of Fe(Zr)					
x	0	0.5010 (28)	0.0029 (71)		1/2
y	0	1/4	1/4		1/2
z	0.2231 (60)	0.0169 (35)	0.5148 (89)		1/2
$B_{eq(Fe)}$(Å^2)	2.75	2.35	2.35		6.05
Position of O					
x	0.4392(46)	0.5	0		1/2
y	0	0	0		1/2
z	0.9545(90)	0	0.5		0
$B_{eq(O)}$(Å^2)	2.58	3.58	3.58		2.81
Position of O					
x		1/4	1/4	0.7789(88)	0.7789(88)	
y	/	1/4	1/4	1/4	1/4	/
z		0.1797(01)	3/4	3/4	0.1797(01)	
$B_{eq(O)}$(Å^2)		3.65	3.65	3.65	3.65	
R_{wp}	0.126	0.181			0.198	
R_{exp}	0.085	0.157			0.168	
R_p	0.100	0.131			0.149	
Gof	1.28	1.15			1.17	
R_{Bragg}	0.053	0.065			0.047	

$c_h = c_H/\sqrt{12}$), a_m, b_m, and c_m in the monoclinic cell ($a_m = a_M/\sqrt{2}$, $b_m = b_M/2$, $c_m = c_M/\sqrt{2}$) for β-phase and a_c in the cubic state for γ-phase, as a function of temperature from 25 °C to 1000 °C, are shown in Fig. 5. An obvious anomaly[22] is observed in the lattice parameters of a_h and c_h at ~400 °C, which corresponds to the Neel temperature and supports the result of DSC. At T_C, the cell parameters a_h and c_h display a sudden and abrupt change, which also induces an important discontinuity in the unit cell volume (inset of Fig. 5). Earlier reports[17,20] have shown that the phase transition at T_C in pure BFO is accompanied by a strong decrease in the volume with a variation $\Delta V/V \approx -1.4\%$. Such strong volume change confirms the first-order nature of the ferroelectric phase transition. Here, in case of BFZ_{95}, the volume at T_C is $\Delta V/V \approx -0.6\%$ which is still strong enough to support the first-order nature of the ferroelectric phase transition. Note that such weaker change compared to that of pure BFO can explain the occurrence of the cubic-like phase in BFZ_{95}. Besides, the new phase transition from β- to γ-phase corresponds to a weak change of the unit cell volume as it goes from 64.13 Å^3 at 890 °C to 64.20 Å^3 at 910 °C (inset of Fig. 5) and, hence, suggests a second-order-like phase transition in agreement with the DSC results.

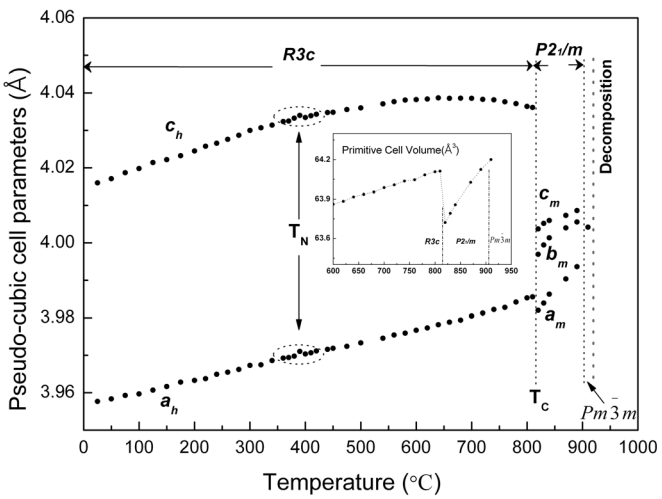

FIG. 5. Temperature-dependence evolution of the $R3c$, the $P2_1/m$, and $Pm\bar{3}m$ cell parameters of BFZ_{95} ceramic described in a pseudocubic cell ($a_h = a_H/\sqrt{2}$, $c_h = c_H/\sqrt{12}$) and $a_m = a_M/\sqrt{2}$, $b_m = b_M/2$, $c_m = c_M/\sqrt{2}$).

IV. DISCUSSIONS

DSC and HTXRD results clearly demonstrate that BFZ_{95} undergoes two phase transitions, i.e., $\alpha \leftrightarrow \beta$ at 815 °C and $\beta \leftrightarrow \gamma$ at 905 °C. The first structural phase transition $\alpha \leftrightarrow \beta$ is confirmed to be of first-order nature, as supported by both temperature hysteresis between exothermic and endothermic peaks in DSC curves and a strong decrease in the unit cell volume ($\Delta V/V \approx -0.6\%$) observed by HTXRD. The crystalline structure to describe the intermediate β phase corresponds to a monoclinic $P2_1/m$ space group, which is different from the orthorhombic *Pbnm* reported by Arnold *et al.*[18] using neutron diffraction techniques. Such discrepancy can be attributed to the fact that oxygen atom positions are better described using neutron diffraction or by the fact that either the Bragg peak intensities are affected by the Bi volatility or some Bragg peaks corresponding to parasitic phases have been considered during the refinement. Note that, in our case, we did not find any decomposition or impure phases in our sample between 820 and 905 °C that may affect the refinement. We believe that Zr-doping stabilizes the perovskite structure of BFO as it allows observing the γ-phase. Besides, the monoclinic phase was also observed between 3.5 and 10 GPa in the recent high pressure experiments of BFO.[31,32] Moreover, contrary to the $\alpha \leftrightarrow \beta$ transition, the second phase transition, i.e., $\beta \leftrightarrow \gamma$, at 905 °C appears to be a second-order-like one as suggested by the DSC data as well as the continuous volume change. We did not find any sharp change in the volume through $\beta \leftrightarrow \gamma$ phase transition in contrast to the result observed in $BiFe_{0.7}Mn_{0.3}O_{3+\delta}$.[25] The highest temperature phase (γ phase) is well described by a cubic $Pm\bar{3}m$ structure, which is evidently supported by the disappearance of super-reflections in the β phase and the symmetric singlet peaks in the diffraction pattern (pattern C in Figs. 3 and 4).

V. CONCLUSIONS

In summary, pure polycrystalline $Bi_{0.95+\delta}Fe_{0.9}Zr_{0.1}O_3$ ceramic has been successfully stabilized by an improved solid-state reaction, through charge compensation ensured by cation vacancies (Bi^{3+}). The pure perovskite ABO_3 phase is obtained thanks to the creation of vacancies on the A site, although the chemical doping was performed on the B site. It highlights that (1) A and B sites of BFO are strongly correlated (2) as a matter of fact, the sub-system FeO is very stable: neither reduction nor oxidation of Fe (III) seems to be possible. As a result, the antiferromagnetic coupling is only weakly affected by such substitution.

$Bi_{0.95+\delta}Fe_{0.9}Zr_{0.1}O_3$ shows the phase transitions sequence: $\alpha \leftrightarrow \beta \leftrightarrow \gamma$. While the symmetry of the intermediate β phase can be described by a monoclinic structure $P2_1/m$. Further work are needed to determine the real structure. In contrast, the concomitant disappearance of the superstructure peaks and the peak splitting is as strong indication for a cubic-like symmetry for the γ-phase appearing at ~905 °C. In addition, we show that the $\alpha \leftrightarrow \beta$ phase transition is clearly of first order, whereas the $\beta \leftrightarrow \gamma$ is more continuous attesting a transition of second-order nature.

ACKNOWLEDGMENTS

We wish to thank Celine Byl for interesting discussions and experimental help. Financial support by the Agence Nationale de la Recherche (PROPER), Natural Science Basis Research Plan in Shaanxi Province of China (Program No.: 2011JM6001), Specialized Research Fund for the Doctoral Program of Higher Education (No.: 20110201120003), China Postdoctoral Science Foundation (Grant No.: 20110491653), and the Fundamental Research Funds for the Central Universities of China (Nos.: XJJ20100148 and 2011JDHZ10) is gratefully acknowledged.

[1] M. Fiebig, J. Phys. D: Appl. Phys. **38**, R123 (2005).
[2] W. Eerenstein, N. D. Mathur, and J. F. Scott, Nature (London) **442**, 759 (2006).
[3] R. Ramesh and N. A. Spaldin, Nature Mater. **6**, 21 (2007).
[4] C. Tabares-Munoz, J. P. Rivera, A. Monnier, and H. Schmid, Jpn. J. Appl. Phys., Suppl. **24**, 1051 (1985).
[5] P. Fischer, M. Polomska, I. Sosnowska, and M. Szymanksi, J. Phys. C **13**, 1931 (1980).
[6] G. A. Smolenskii and I. Chupis, Sov. Phys. Usp. **25**, 475 (1982).
[7] F. Kubel and H. Schmid, Acta Crystallogr., Sect. B: Struct. Sci. **46**, 698 (1990).
[8] I. Sosnowska, T. Peterlin-Neumaier, and E. Steichele, J. Phys. C **15**, 4815 (1982).
[9] I. Sosnowska and A. K. Zvezdin, J. Magn. Magn. Mater. **140**, 167 (1995).
[10] M. M. Kumar, V. R. Palkara, K. Srinivas, and S. V. Suryanarayana, Appl. Phys. Lett. **76**, 8 (2000).
[11] J. Wang, J. B. Neaton, H. Zheng, V. Nagarajan, S. B. Ogale, B. Liu, D. Viehland, V. Vaithyanathan, D. G. Schlom, U. V. Waghmare, N. A. Spaldin, K. M. Rabe, M. Wuttig, and R. Ramesh, Science **299**, 1719 (2003).
[12] M. K. Singh, S. Ryu, and H. M. Jang, Phys. Rev. B **72**, 132101 (2005).
[13] J. T. Wu, S. Y. Mao, Z. G. Ye, Z. X. Xie, and L. S. Zheng, J. Mater. Chem. **20**, 6512 (2010).
[14] R. Haumont, J. Kreisel, P. Bouvier, and F. Hippert, Phys. Rev. B **73**, 132101 (2006).
[15] A. Maitre, M. Francois, and J. C. Gachon, J. Phase Equilib. **25**, 59 (2004).
[16] S. M. Selbach, T. Tybell, M. A. Einarsrud, and T. Grande, Adv. Mater. **20**, 3692 (2008).
[17] R. Palai, R. S. Katiyar, H. Schmid, P. Tissot, S. J. Clark, J. Robertson, S. A. T. Redfern, G. Catalan, and J. F. Scott, Phys. Rev. B **77**, 014110 (2008).
[18] D. C. Arnold, K. S. Knight, F. D. Morrison, and P. Lightfoot, Phys. Rev. Lett. **102**, 027602 (2009).
[19] I. A. Kornev, S. Lisenkov, R. Haumont, B. Dkhil, and L. Bellaiche, Phys. Rev. Lett. **99**, 227602 (2007).
[20] R. Haumont, I. A. Kornev, S. Lisenkov, L. Bellaiche, J. Kreisel, and B. Dkhil, Phys. Rev. B **78**, 134108 (2008).
[21] A. G. Gavriliuk, V. V. Struzhkin, I. S. Lyubutin, M. Y. Hu, and H. K. Mao, JETP Lett. **82**, 224 (2005).
[22] G. Catalan and J. F. Scott, Adv. Mater. **21**, 2463 (2009).
[23] Q. H. Jiang, F. T. Liu, C.-W. Nan, Y.-H. Lin, M. J. Reece, H. X. Yan, H. P. Ning, and Z. J. Shen, Appl. Phys. Lett. **95**, 012909 (2009).
[24] A. Singh, J. P. Patel, and D. Pandey, Appl. Phys. Lett. **95**, 142909 (2009).
[25] S. M. Selbach, T. Tybell, M. A. Einarsrud, and T. Grande, Phys. Rev. B **79**, 214113 (2009).
[26] J. Wei, R. Haumont, R. Jarrier, P. Berhtet, and B. Dkhil, Appl. Phys. Lett. **96**, 102509 (2010).
[27] J. F. Bérar, in Satellite Meeting of IUCr. on Powder Diffractometry, Toulouse, France, 1990.
[28] Y. P. Wang, L. Zhou, M. F. Zhang, X. Y. Chen, J. M. Liu, and Z. G. Liu, Appl. Phys. Lett. **84**, 1731 (2004).
[29] X. D. Qi, J. Dho, R. Tomov, M. G. Blamire, and J. L. MacManus-Driscoll, Appl. Phys. Lett. **86**, 062903 (2005).
[30] *International Tables for Cyrstallography*, edited by A. J. C. Wilson (Kluwer, Dordrecht, 1992).
[31] R. Haumont, P. Bouvier, A. Pashkin, K. Rabia, S. Frank, B. Dkhil, W. A. Crichton, C. A. Kuntscher, and J. Kreisel, Phys. Rev. B **79**, 184110 (2009).
[32] M. Guennou, P. Bouvier, G. S. Chen, B. Dkhil, R. Haumont, G. Garbarino, and J. Kreisel, Phys. Rev. B **84**, 174107 (2011).